

Double-Disordered HTS-Coated Conductors and Their Assemblies Aimed for Ultra-High Fields: Large Area Tapes

Alexander Usoskin¹, Ulrich Betz, Frank Hofacker, Alexander Rutt, Klaus Schlenga, Burkhard Prause, Lucio Rossi², Luca Bottura, Amalia Ballarino, Carmine Senatore³, Anna Kario, Wilfried Goldacker, Alexander Meledin⁴, Dmytro Abramov⁵, and David Larbalestier⁶

Abstract—Double disordered (DD) HTS layers processed via high-fluence PLD with modulated pressure and barium zirconate precipitation yield very high engineering current densities, above 900 and 600 A/mm² at 18 and 31 T, respectively, measured at 4.2 K and $B \parallel c$. Tape architecture is based on 50–100- μm -thick polished stainless steel tape which prior to DD-HTS deposition was coated with YSZ template yielding a biaxial in-plane texture with FWHM = 10–11° characterized using phi-scan XRD technique. High-resolution nanostructural analysis indicated a number of nonusual features in DD YBCO layers regarding “firework”-like orientation of nanoprecipitations/nanochains. These new features result in a very high concentration of local defects which reduce the critical current (I_c) measured at 77 K, self-field to about 30% of the corresponding I_c in non-DD YBCO, and simultaneously lead to substantial gaining of I_c at high fields. The main result is a substantial improvement of I_c and engineering current density (J_e) achieved at high field and liquid Helium temperature in long length, large area tapes with 4 and 12 mm width. J_e above 970 A/mm² at 4.2 K, $B = 18$ T, $B \parallel c$ was achieved in 12-mm-wide tape.

Index Terms—High-temperature superconductors, superconducting tapes, yttrium compounds, laser ablation, epitaxial growth, doping, superconducting materials.

I. INTRODUCTION

DDOUBLE disordered high temperature superconductor (DD-HTS) coated tapes incorporating both an extrinsic

Manuscript received September 19, 2017; accepted January 30, 2018. Date of publication February 2, 2018; date of current version May 10, 2018. This work was supported in part by the European Commission (EC) through FP7-EuCARD2 under Grant 312453 and in part by the CERN together with EC through program H2020-ARIES, as well as EU-FP7 NMPLA-2012-280432 EUROTAPES project. (Corresponding author: Alexander Usoskin.)

A. Usoskin, U. Betz, F. Hofacker, A. Rutt, K. Schlenga, and B. Prause are with the Bruker HTS GmbH, Alzenau 63755, Germany (e-mail: alexander.usoskin@bruker.com; ulrich.betz@bruker.com).

L. Rossi, L. Bottura, and A. Ballarino are with CERN, Genève 1211, Switzerland.

C. Senatore is with the University of Genève, Genève 4 CH-1211, Switzerland.

A. Kario and W. Goldacker are with the KIT ITEP, Karlsruhe 76344, Germany.

A. Meledin was with the University of Antwerp, Antwerpen 2000, Belgium. He is now with RWTH University of Aachen, Aachen 52062, Germany.

D. Abramov and D. Larbalestier are with the Applied Superconductivity Center, National High Magnetic Laboratory, Tallahassee, FL 32310 USA.

Color versions of one or more of the figures in this paper are available online at <http://ieeexplore.ieee.org>.

Digital Object Identifier 10.1109/TASC.2018.2801348

and intrinsic nano-structural disorder are characterized by very high in-field critical currents. In DD-HTS, a superimposing of intrinsic and extrinsic disorder takes place in a way that (i) the intrinsic disorder is caused by local stoichiometry deviations that lead to defects of crystallinity that serve as pinning centers in the $\text{YBa}_2\text{Cu}_3\text{O}_{x-\delta}$ (YBCO) matrix and (ii) the extrinsic disorder is introduced via embedded atoms or particles of foreign material (e.g., barium zirconate, BZO). To a large extent, the advanced currents are due to large concentration of local defects of crystallinity generated in DD-HTS coated tapes. High in-field critical currents gained by DD-like architectures in comparison with alternative HTS nano-architectures [1], [2] made a substantial impact to recent progress in upgraded technologies of long HTS coated tapes [3], [4] based on pulsed-laser-deposition (PLD) [5], [6]. In 2017, the EUROTAPES EC project was successfully finalized in large part thanks to a PLD progress at Bruker resulted in processing of >500 m long HTS coated tapes (project goal) [6]–[8]. Nearly at the same time, an improvement of engineering critical current density, J_e , above 700 A/mm² at 4.2 K, 18 T and $B \parallel c$ was reported by Bruker within EUCARD2, CERN [7], [9]. This result was obtained in up-scaled PLD system capable of deposition of 180 m length of 12 mm wide tape. Long scale tapes with sufficient currents aimed for operation in medium field magnets at 20 K were demonstrated recently by Fujikura and partners [5], [10], [11]. SuperOx reported also successful steps in upscaling of PLD technology [2], [11].

Key aim of the up-scaling is to provide high current tapes for high-field magnets (>20 T) operating at 4.2 K as well as high-field motors, SMES devices and NMR/MRI operating at >20 K. In all these cases, HTS coated conductors with respect to alternative superconductors and normal metals demonstrate clear advantages in combination of their high J_e level and sufficient mechanical stability.

Substantial progress was done in this direction also by Bruker HTS in the recent past. A significant increase of critical current in the high magnetic field, up to 31 T, was observed in tapes manufactured by employing a double-disorder (DD) route [3], [8] which creates a set of lattice defects [12]–[14] in the HTS layer.

Presently we report a new study on large area DD-deposition, nano-morphology of the DD-HTS layers, and present an updated status of long-length tape processing including recent characterization of critical currents in fields up to 31 T.

II. PROCESSING TECHNOLOGY

A. Tape Processing Steps

Cr–Ni stainless steel tapes, 100 μm thick, 4 mm or 12 mm wide, were employed as a substrate tape after precise nano-polishing which enables a surface roughness <5 nm (determined with 100 nm \times 100 nm surface area). The substrate yields a 650–670 MPa tensile strength (at 20 $^\circ\text{C}$) which plays an essential role in high field applications.

HTS layers with double disordered structure were deposited via pulsed laser deposition (PLD) technique onto metallic substrate tapes [3] coated with yttria-stabilized zirconia (YSZ) template fabricated using an alternating-beam-assisted deposition (ABAD) [14] and, finally, with ceria (CeO_2) cap layer [3], [15]. The ABAD-YSZ layer fabricated with a thickness of 1.7–2.6 μm represented a template with in-plane texture which corresponds to a full-width at half-maximum (FWHM) of 9 $^\circ$ –10 $^\circ$ (ϕ -scan). Such bi-axially textured buffer layer represents a template for crystalline orientation of further layers to be grown.

Further layers are a 0.05–0.1 μm thick ceria cap layer, and a 1.5–2 μm thick $\text{YBa}_2\text{Cu}_3\text{O}_{x-\delta}$ (YBCO) layer. Both of them were deposited employing a multibeam pulsed laser deposition method described elsewhere [3]. Superimposing of two different ways for “disordering” of DD-YBCO mentioned above was enabled via (i) local perturbation of intrinsic HTS stoichiometry and (ii) extrinsic precipitation with barium zirconate (BZO). Earlier [3] we listed some specific features of film growth which differentiate the employed PLD method from other methods. These are (i) a drum-based tape transport, (ii) equilibrium heating (QEH) which provides a “hot-wall reactor” in the deposition zone [16], (iii) quick substrate/drum rotation combined with creation of movable deposition zone via laser beam scans and (iv) oscillations of oxygen pressure during PLD. It was shown that PLD technique based on such features enables deposition of HTS films with advanced in-field performances [3]. A view of the up-scaled deposition machine (PLD-600) is shown in Fig. 1. Another “large area” PLD machine, the PLD-300 (capable of deposition onto 300 m of 4 mm wide tape) was installed with participation of CERN mainly for processing of 12 mm wide tapes.

The end steps of tape processing include [3] (a) an oxygen post-loading performed at about 450–500 $^\circ\text{C}$, (b) double side vacuum metallization with 1–2 μm thick silver layer deposited by vacuum thermal evaporation, and (c) galvanic plating with 20–40 μm thick Cu layer.

B. Large Scale PLD

Study of pulsed laser deposition (PLD) in large area application had shown a substantial influence of lateral flows of laser plume which propagate near to the substrate surface when high laser beam fluence (>8 J/cm 2) is employed [4].

A schematic view of propagation of laser plume between target 1 and substrate 2 is reported in Fig. 2. The plume induced by laser beam 3 contains normal 5 and lateral plasma flows 6. Lateral flows 6 are obviously “guided” by substrate surface which has to be sufficiently large. In Fig. 2(b) is depicted a

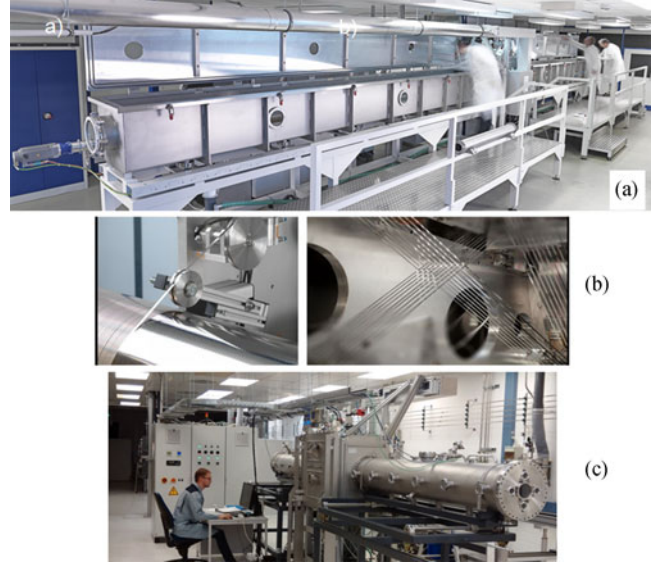


Fig. 1. (a) View of up-scaled PLD machine capable of HTS layer deposition onto 600 m long, 4 mm wide tapes (PLD-600). This equipment is based on drum tape carrier. Quick rotation of the tape with drum enables homogeneity of HTS layer. LSX-200 excimer laser used as a source beam with $\lambda = 308$ nm and up to 300 Hz pulse repetition rate is employed for laser ablation. (b) Alternative reel-to-reel technique employed in processing. (c) View of PLD-300 machine aimed for deposition of 300 m long, 4 mm wide tapes or 100 m long, 12 mm wide tapes for CERN magnets.

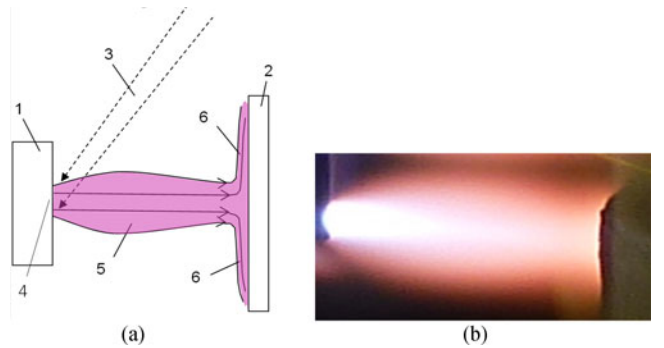


Fig. 2. (a) A schematic view of propagation of laser plume between target 1 and substrate 2. The plume induced by laser beam 3 impinging target spot 4 contains normal 5 and lateral plasma flows 6. Lateral flows 6 are obviously “guided” by substrate. (b) Photoimage of single laser plume coming from target (left side) to the substrate (from the right) where a “nucleation” area of lateral flow is visible.

photo-image of single laser plume coming from the target (left side) to the substrate (from the right) where a “nucleation” area of lateral flow is visible. Distribution of thickness observed on large area substrate is shown with squares in Fig. 3 at high fluence of 9 J/cm 2 . Distribution function is well approximated by sum of Gaussian distributions:

$$f(z, z_0) = C_0 \left\{ \exp \left[- \left(\frac{z - z_0 + \delta}{\sqrt{2}\sigma} \right)^2 \right] + \exp \left[- \left(\frac{z - z_0 - \delta}{\sqrt{2}\sigma} \right)^2 \right] \right\} \quad (1)$$

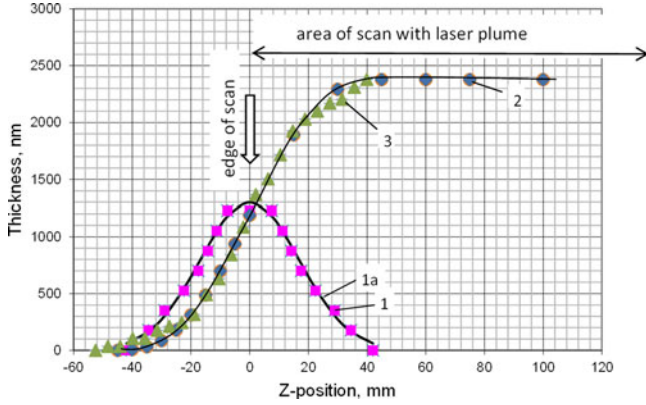


Fig. 3. Thickness distribution of YBCO layer deposited with stationary laser plume centered at $z = 0$ (squares) and linearly scanned substrate with laser plume within z from 0 to 150 mm (triangles). Curve 1a has been calculated with equation (1) using $\sigma = 16$ mm, $\delta = 2$ mm and fitted C_0 . Curve and circles 2 have been calculated via equation (2) with $z_1 = 150$ mm, $C_1 \cdot C_0 = 29 \times 10^{-6}$.

where σ is a standard width of distribution, δ is a split distance between two components of the distribution, z_0 defines the center of the distribution and C_0 is defined in units of length. Eq. (1) describes sufficiently well (curve 1a) thickness experimental distribution 1 in Fig. 3. Split of two Gaussian distributions in (1) allows to describe a self-etching effect which may result in local concave area at $z = 0$. This effect is visible from experimental dependence 1 (squares) in Fig. 3 as a “flattening” of central maximum.

In case when linear scan of the substrate with laser plume is performed in a way that end-position of the plume is by $z = 0$, film thickness distribution is given by the following integral:

$$F(z) = C_1 \cdot \int_0^{z_1} f(z, z_0) dz_0. \quad (2)$$

Parameters used in calculations are in the caption of Fig. 3.

Presence of lateral flows by pulsed laser deposition performed at high fluence allows to qualify such deposition process as well-known “off-axis” deposition [18]–[20] where direction of initial laser plume is parallel to the substrate. In our case this is valid for lateral flows which appear due to deflection of initial laser plume by substrate surface. Interesting fact here is that thickness distribution analyzed in two orthogonal direction shows no influence of substrate curvatures (at least by radii of ~ 100 mm). This obviously means that at certain conditions the plasma/molecular flow is as “guided” by substrate surface.

Effective area of “on-axis” deposition corresponds to 7–10 mm radius in the stationary thickness distribution 1 in Fig. 3. This area is defined via minimal radius r_0 of plume aperture diaphragm which still does not disturb the thickness distribution $t(z)$. This diaphragm through which laser plume spreads towards the substrate was installed at ~ 10 mm distance from the substrate. Amount of material $dm(z)$ deposited within different radial zones may be determined as $dm(z) = 2\pi\rho \cdot z \cdot t(z) \cdot dz$, where ρ is the density of the layer and z values are assumed to be not negative. Integration of this equation shows that “on-axis” area contains only 10–20% of totally deposited film

material (consider that due to cylindrical symmetry $dm(0) = 0$ and maximum of $dm(z)/dz$ is reached at $z \sim 20$ mm. Respectively, the major part of deposited material, up to 90%, is transported by lateral flow. Thus the method may be called as Lateral-Flow Pulsed-Laser-Deposition (LF-PLD).

Advanced quality films deposited via off-axis PLD may explain the success of high fluence PLD in processing of HTS layers [1]–[5]. On the other hand, disadvantage of off-axis PLD regarding substantial losses of incoming material [19], [20] is not valid for high-area PLD where the lateral flows are employed in film deposition.

Obviously LF-PLD may cause a number of specific structural and HTS features part of which is considered in the next section.

III. NANO-MORPHOLOGY

A. Nano-Structure of DD-HTS Layer

High-resolution scanning transmission electron microscopy (STEM), energy dispersive X-ray spectroscopy (EDX) and other nano-structural analytic means indicated a number of non-usual features in DD YBCO layers: (i) variable angle of second phase columns based on position in the YBCO grain, (ii) presence of in-plane ordered of some fraction of this inclusions, (iii) very small (below 4 nm) size of nano-dots, and (iv) axial symmetry of column assemblies within a single YBCO crystallite that represents a typical nano-structure of major part of other crystallites. These new features result in a very high concentration of local defects which reduce the critical current (I_c) measured at 77 K, self-field (SF) to about 30% of the corresponding I_c in non-DD YBCO, and simultaneously lead to substantial gaining of I_c at high fields, as well as relatively weak anisotropy.

Main features that follow from Fig. 4 may be summarized as

- precipitation chains are relatively long (>500 nm),
- precipitation chains are oriented conically diverging with increasing distance from the substrate; the chains are tilted out of the axis creating the “flowers bouquet” or the “fireworks” morphology (see dash lines in Fig. 4 (b)). This is especially obvious when observed along the normal to the substrate surface,
- intrinsic disorder is observed as horizontal insertions [3],
- BZO filling is represented as bamboo structures where the BZO chains may bend up to horizontal orientation (see Fig. 4 (a), (c) and (d)),
- the planar structures are built by agglomerates of precipitation nanoparticles; in many cases they are formed as a result of bending of “vertical” chains,
- high density of precipitation chains with small distance between them (<15 nm) and diameter of chain <6 nm are observed (Fig. 4) and in [3].

B. Self-Etching

Distribution of kinetic energy of ions in laser plume [21] is very wide and can reach relatively high energies of 200 eV that are sufficient for efficient re-sputtering which starts already from 20–30 eV thresholds [22]. In our process the self-etching

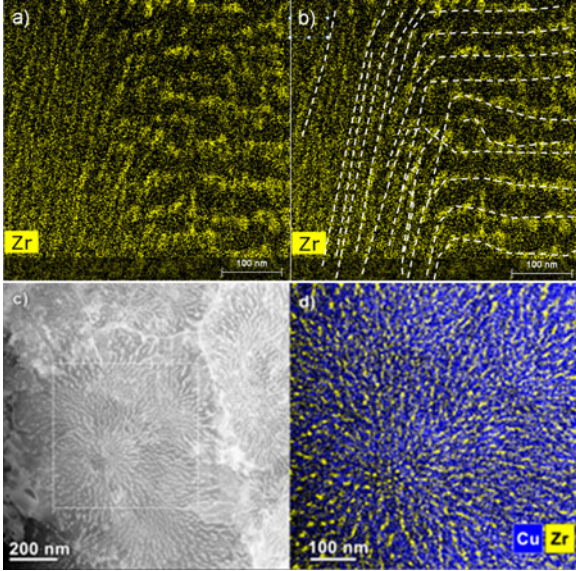


Fig. 4. ADF STEM image (c) and EDX maps (a), (b), and (d) indicating distribution of Zr (in yellow) and Cu (in blue), (d) corresponds to marked area in (c), (a) and (b) represent nano-column/bamboo chains of precipitation where tracing of the chains is indicated with white dash-curves [which serve for clarification of image shown in (a)]. (a) and (b) correspond to cross-sectional view. (c) and (d) – planar views, i.e., views in normal direction to the film surface.

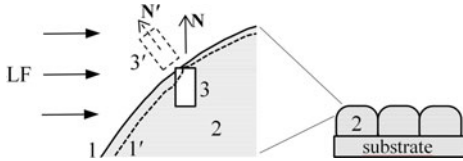


Fig. 5. Schematic steps of re-sputtering and further growth for convex segment 1, 1' of crystallite 2 with embedded nano-particles 3, 3' under influence of lateral flow LF. Normals N and N' indicate growth direction of 3 and 3'.

is obviously responsible for flattening of center of thickness distribution 1 in Fig. 3.

Inclined precipitation formed as nano-chains were already shown with much thicker BZO columns by other works; see e.g., [10], [26]. In our case, we observe such wide variety of angles that possibly was not observed so far. We tried to investigate the origin of the fine structure we deal with.

The most probable interpretation of growth mechanism is related to self-etching (self-re-sputtering) of the surface 1 of YBCO crystallite 2 with lateral ion flow LF. A simplified schema of this process is shown in Fig. 5 where a segment of the crystallite 2 with convex surface 1 is depicted. According to employed model a number of sequential discrete steps of growth and re-sputtering approximates the LF deposition process. Because of difference in re-sputtering yield for YBCO matrix and BZO particles a re-sputtering step changes an orientation of normal from N to N' due to change of surface shape from 1 to 1' (see Fig. 5). This should further cause a change of growth direction of next BZO element 3' towards more “oblique” orientation at the following growth step. Such consideration may be generalized for the cases of non-central cross-section of the crystallite and random orientation of lateral flow, in both cases without basic change of resulting effect [4]. Thus considered mechanism

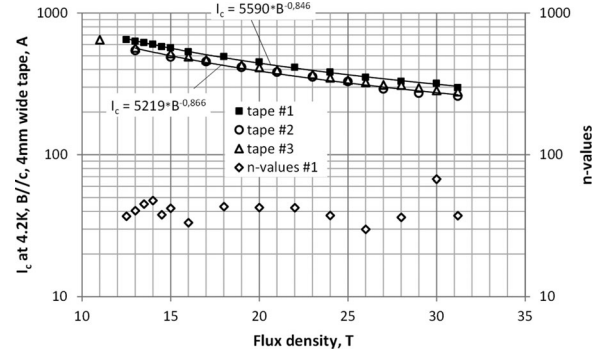


Fig. 6. Critical current vs. flux density, B , measured in the end pieces (#1, #2) of 500–600 m long, 4 mm wide tapes, and end-reference sample (#3). Squares, triangles, and circles correspond to “transport” I_c values and rhombs indicate n -values for sample #1 measured at 4.2 K, $B \parallel c$ (Tallahassee, June, 2017).

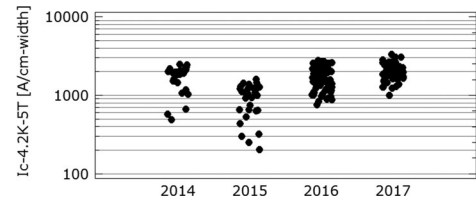


Fig. 7. Progress in improvement of in-field critical current. Current I_c is measured in end pieces of 500 m long, 4 mm wide tapes at 4.2 K, 5 T, $B \parallel c$.

can explain a radial orientation and an axial symmetry of the nano-structure within a single grain (see Fig. 4(c), (d)).

IV. HTS COATED TAPES: STATUS

A. Critical Currents and Current Densities

Critical current I_c as a function of flux density, B , measured in the end pieces of 500–600 m long tapes and end-reference sample are shown in Fig. 6. Tapes, 4 mm wide, are deposited in accordance with technology described above. Mean n -values of measured samples correspond to ~ 40 . Average alpha value representing an exponents in $I \sim B^{-\alpha}$ function equals approximately to 0.856 ± 0.010 . High-field measurements were performed at 4.2 K, $B \parallel c$ at Tallahassee in June, 2017. Progress in improvement of critical current is depicted in Fig. 7. Current I_c was measured in end pieces of 4 mm wide tapes at 4.2 K, 5 T, $B \parallel c$. Progress in improvement of engineering critical current density, J_e , in sequence of 12 mm wide tapes processed in batches of 30–90 m is demonstrated in Fig. 8. Measurements are performed for the end and intermediate tape-pieces at 18 and 5 T, $B \parallel c$, 4.2 T. Some $J_e - s$ were evaluated for the α -values derived from the curves shown in Fig. 6 (both tapes with 4 and 12 mm width exhibit similar in-field behavior). The highest J_e recorded at 18 T was about 970 A/mm^2 .

B. I_c Homogeneity

Distribution of critical current, $I_c(x)$, measured across a 550 m long, 4 mm wide tape is shown in Fig. 9 (x is a longitudinal coordinate). Transport current was measured both at 77 K, SF and 4.2 K, 5 T, $B \parallel c$. TapeStar scan performed with Hall arrays at SF, 77 K (Fig. 9(b)) is in a good agreement with transport I_c at

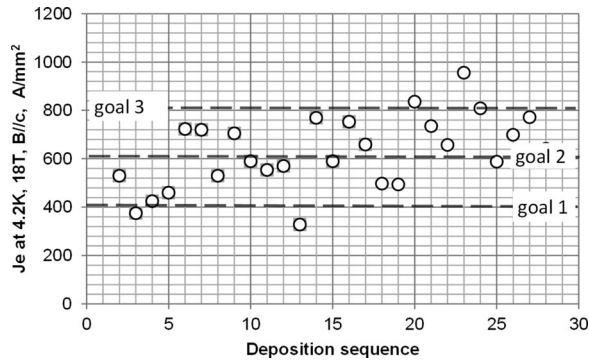


Fig. 8. Engineering critical current density J_e in sequence of 12 mm wide tapes processed in batches of 30–90 m. Measurements are performed in end and intermediate tape pieces at 18 and 5 T, $B \parallel c$, 4.2 T. Highest J_e corresponds to 970 A/mm^2 .

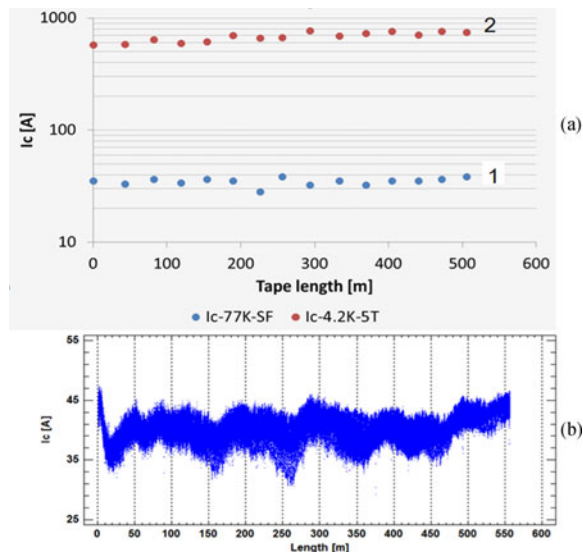


Fig. 9. Critical current distribution measured along a 550 m long tape via (a) transport current measurements at 77 K, SF (circles 1) and 4.2 K, 5 T, $B \parallel c$ (circles 2) in 4 mm wide tape and (b) TapeStar scan. I_c – s at 77 K are relatively low because of high lift factors.

77 K. Lift factors between I_c – s at 4.2 K, 5 T, $B \parallel c$ and 77 K, SF are rather high, from ~ 17 to 40 (see next section). Thus I_c – s at 77 K are relatively low. Effect of “anti-correlation” of “in-field” and “ex-field” critical current was observed where a local minimum in $I_c(x)$ at 77 K, SF corresponds to a maximum of $I_c(\geq 5 \text{ T}, 4.2 \text{ K})$ located at the same x -position. In many cases, this effect leads to an improvement of homogeneity of I_c at $B \geq 5 \text{ T}, 4.2 \text{ K}$.

C. Lift-Factor

Dependence of I_c (18 T, $B \parallel c$, 4.2 K) versus I_c (SF, 77 K) is shown in Fig. 10. Ratio of these currents represents a lift factor, LFA, which in our tapes may exceed 15 as it follows from Fig. 10. The lift factor lines in Fig. 10 indicate that our tapes are mainly within lift factors of 7 to 16.

At $B = 5 \text{ T}$ lift factors are approximately 2.5 times higher. Thus they are mostly in the range from 17 to 40. It is interesting to see that there is no good correlation between high level I_c and lift factor. In Fig. 10, for example, highest in-field I_c may equally

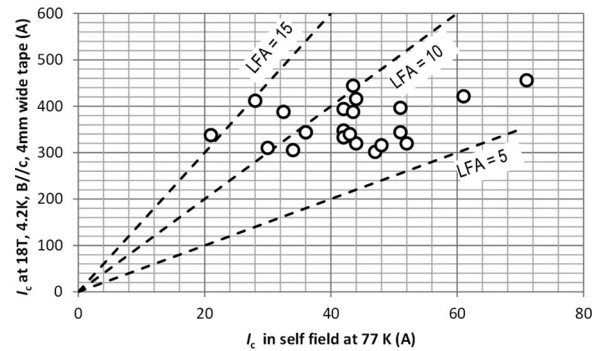


Fig. 10. I_c (18 T, $B \parallel c$, 4.2 K) versus I_c (SF, 77 K). Ratio of these currents represents a lift factor.

be reached by “ex-field” I_c varying from 28 to 50 A, i.e., within practically the whole range observed by us. This additionally confirms the fact that correlation between these two I_c – s is hard to find [3].

C. BRIEF SUMMARY

PLD based on lateral flow (LF) is established using a high fluence laser ablation.

LF-PLD results in nano-morphology of ordered Zr based nano-chains exhibits a wide angular divergence looking as a firework. The chains may be turned from vertical to horizontal orientation. This may results in higher isotropy of in-field performance of DD-HTS layers.

ABAD/DD-PLD technology up-scaled to 600 m tape length yields very high currents, e.g., up to 290 A in 4 mm wide tape at 30 T, 4.2 K, $B \parallel c$. In 12 mm wide tapes, a $J_e = 970 \text{ A/mm}^2$ is achieved as best value at total tape thickness of 0.14 mm. Anti-correlation effect is found in I_c distributions along the tape length measured at 77 K, self-field and 4.2 K, 5 T, $B \parallel c$.

ACKNOWLEDGMENT

The authors acknowledge the support of high-field measurements provided via established project by National High Magnetic Field Laboratory in Tallahassee and the technical support of ultra-high field measurements provided by Griffin Bradford, ASC FSU, NHMFL, Tallahassee, FL.

REFERENCES

- [1] Y. Iijima *et al.*, “Development for mass production of homogeneous RE123 coated conductors by hot-wall PLD process on IBAD template technique,” *IEEE Trans. Appl. Supercond.*, vol. 25, no. 3, Jun. 2015, Art. no. 6604104. doi: [10.1109/TASC.2014.2379923](https://doi.org/10.1109/TASC.2014.2379923).
- [2] S. Samoilonkov *et al.*, “Customised 2G HTS wire for applications,” *Supercond. Sci. Technol.*, vol. 29, 2016, Art. no. 024001 (10p). doi: [10.1088/0953-2048/29/2/024001](https://doi.org/10.1088/0953-2048/29/2/024001).
- [3] D. Abraimov *et al.*, “Double disordered YBCO coated conductors of industrial scale: High currents in high magnetic field,” *Supercond. Sci. Technol.*, vol. 28, 2015, Art. no. 114007 (8p). doi: [10.1088/0953-2048/28/11/114007](https://doi.org/10.1088/0953-2048/28/11/114007).
- [4] A. Usoskin *et al.*, “Artificial pinning centers in long length HTS coated conductors,” *Supercond. Sci. Technol.*, to be published.
- [5] Y. Iijima, K. Kakimoto, M. Igarashi, S. Fujita, and S. Awaji, “BMO doped REBCO coated conductors for uniform in-field by hot-wall PLD process using IBAD template,” *IEEE Trans. Appl. Supercond.*, vol. 27, no. 4, Jun. 2017, Art. no. 6602804. doi: [10.1109/TASC.2017.2660305](https://doi.org/10.1109/TASC.2017.2660305).

- [6] European team announces superconductivity breakthrough. [Online]. Available: <https://phys.org/news/2017-03-european-team-superconductivity-breakthrough.html>
- [7] A. Usoskin, U. Betz, F. Hofacker, R. Dietrich, and K. Schlenga, "Long HTS tapes with high in-field performance manufactured via multibeam PLD with "Dynamic" drum concept," *IEEE Trans. Appl. Supercond.*, vol. 27, no. 4, Jun. 2017, Art. no. 6600605.
- [8] A. Usoskin, U. Betz, R. Dietrich, and K. Schlenga, "Long HTS coated conductor processed via large-area PLD/ABAD for high-field applications," *IEEE Trans. Appl. Supercond.*, vol. 26, no. 3, Apr. 2016, Art. no. 6602304. doi: [10.1109/TASC.2016.2542253](https://doi.org/10.1109/TASC.2016.2542253).
- [9] G. A. Kirby *et al.*, "First cold powering test of REBCO Roebel wound coil for the EuCARD2 future magnet development," *IEEE Trans. Appl. Supercond.*, vol. 27, no. 4, Jun. 2017, Art. no. 4003307.
- [10] S. Miura *et al.*, "Improvement in J_c performance below liquid nitrogen temperature for $\text{SmBa}_2\text{Cu}_3\text{O}_y$ superconducting films with BaHfO_3 nanorods controlled by low-temperature growth," *APL Materials*, vol. 4, 2016, Art. no. 016102. doi: [10.1063/1.4939182](https://doi.org/10.1063/1.4939182).
- [11] J. Fleiter, K. Konstantopoulou, D. Richter, and A. Ballarino, "Characterization of REBCO tape and Roebel cable at CERN," presented at the 4th Workshop of the Series Accelerator Magnets in High Temperature Superconductors, Barcelona, 15th Feb. 2017. [Online]. Available: https://indico.cern.ch/event/588810/contributions/2409890/attachments/1416093/2168137/6_-_Characterization_of_REBCO_Tape_and_Cable_at_CERN_WAMHTS_2017.pdf, Accessed on Sep 06, 2017
- [12] D. Larbalestier, A. Gurevich, D. M. Feldmann, and A. Polyanskii, "High- T_c superconducting materials for electric power applications," *Nature (London)*, vol. 414, p. 368, 2001. doi: [10.1038/35104654](https://doi.org/10.1038/35104654).
- [13] V. Selvamanickam, M. Heydari Gharahcheshmeh, A. Xu, E. Galstyan, L. Delgado, and C. Cantoni, "High critical currents in heavily doped $(\text{Gd},\text{Y})\text{Ba}_2\text{Cu}_3\text{O}_x$ superconductor tapes," *Appl. Phys. Lett.*, vol. 106, p. 032601, 2015. doi: <http://dx.doi.org/10.1063/1.4906205>.
- [14] P. Mele, S. J. Singh, S. Saini, A. K. Jha, and M. I. Adam, "Nanostructured oxide thin films for sustainable development," *Procedia Eng.*, vol. 171, 2017, pp. 201–206. doi: [10.1016/j.proeng.2017.01.327](https://doi.org/10.1016/j.proeng.2017.01.327).
- [15] A. Usoskin and L. Kirchhoff, "In-plane texturing of buffer layers by alternating beam assisted deposition: Large area and small area applications," *Mater. Res. Soc. Symp. Proc.*, vol. 1150, pp. 117–122, 2009.
- [16] A. Usoskin and H. C. Freyhardt, "YBCO-coated conductors manufactured by high-rate pulsed laser deposition," *MRS Bull.*, vol. 29, pp. 583–589, 2004.
- [17] U. P. Bansode and S. Ogale, "On-axis pulsed laser deposition of hybrid perovskite films for solar cell and broadband photo-sensor applications," *J. Appl. Phys.*, vol. 121, Apr. 2017, Art. no. 133107. doi: [10.1063/1.4979865](https://doi.org/10.1063/1.4979865).
- [18] C. L. Veenas, K. M. Nissamudeen, S. L. Smitha, V. Biju, and K. G. Gopchandran, "Off-axis PLD: A novel technique for plasmonic engineering of silver nanoparticles," *J. Optoelectronics Adv. Mater.*, vol. 11, no. 2, pp. 114–122, Feb. 2009.
- [19] V. Boffa *et al.*, "High-quality YBCO thin films grown by off-axis PLD geometry," *IEEE Trans. Appl. Supercond.*, vol. 7, no. 2, pp. 1189–1192, Jun. 1997. doi: [10.1109/77.620711](https://doi.org/10.1109/77.620711).
- [20] B. C. Min, Y. H. Choi, S. H. Moon, S. M. Lee, S. Y. Lee, and B. Oh, "Double-sided $\text{YBa}_2\text{Cu}_3\text{O}_{7-\delta}$ thin films made by off-axis pulsed laser deposition," *Supercond. Sci. Technol.*, vol. 14, no. 8, pp. 543–547, Jul. 2001.
- [21] G. C. Tyrrell, L. G. Coccia, T. H. York, and I. W. Boyd, "Energy-dispersive mass spectrometry of high energy ions generated during KrF excimer and frequency-doubled Ng:YAG laser ablation of metals," *Appl. Surface Sci.*, vol. 96, pp. 227–232, 1996.
- [22] C. Yan and Q. Y. Zhang, "Study on low-energy sputtering near the threshold energy by molecular dynamics simulations," *AIP Adv.*, vol. 2, 2012, Art. no. 032107. doi: [10.1063/1.4738951](https://doi.org/10.1063/1.4738951).
- [23] S. S. Yap, Ch. H. Nee, S. L. Yap, and T. Y. Tou, "Nanostructured diamond-like carbon films grown by off-axis pulsed laser deposition," *J. Nanomaterials*, vol. 2015, 2015, Art. no. 731306 (6p). doi: [10.1155/2015/731306](https://doi.org/10.1155/2015/731306).